Contact Angles on a Soft Solid: From Young's Law to Neumann's Law

Antonin Marchand,[1] Siddhartha Das,[2,*] Jacco H. Snoeijer,[2] and Bruno Andreotti[1]

[1]*Physique et Mécanique des Milieux Hétérogènes, UMR 7636 ESPCI-CNRS, Université Paris-Diderot, 10 rue Vauquelin, 75005 Paris, France*

[2]*Physics of Fluids Group and MESA+Institute for Nanotechnology, University of Twente, P. O. Box 217, 7500 AE Enschede, The Netherlands*

(Received 13 May 2012; revised manuscript received 18 September 2012; published 5 December 2012)

The contact angle that a liquid drop makes on a soft substrate does not obey the classical Young's relation, since the solid is deformed elastically by the action of the capillary forces. The finite elasticity of the solid also renders the contact angles differently from those predicted by Neumann's law, which applies when the drop is floating on another liquid. Here, we derive an elastocapillary model for contact angles on a soft solid by coupling a mean-field model for the molecular interactions to elasticity. We demonstrate that the limit of a vanishing elastic modulus yields Neumann's law or a variation thereof, depending on the force transmission in the solid surface layer. The change in contact angle from the rigid limit to the soft limit appears when the length scale defined by the ratio of surface tension to elastic modulus γ/E reaches the range of molecular interactions.

DOI: 10.1103/PhysRevLett.109.236101 PACS numbers: 68.03.Cd

The wetting of liquid drops on deformable solids is important in many circumstances, with examples from biology to microfluidic devices [1–4]. When the solid is soft or flexible, the shapes of both the solid and the liquid are determined by elastocapillary interactions, i.e., by the elastic response to the capillary forces [5,6]. The resulting surface deformations have major consequences for the condensation of drops on soft solids [7], as used for micropatterning of polymeric surfaces [8], mechanical stability of gels [9], or wetting on very soft coatings. To date, however, the most basic characterization of wetting has remained elusive for highly deformable solids [10–13]: What is the contact angle that a liquid makes on a soft solid?

The geometry of the interfaces near the three-phase contact line is governed by two classical laws that describe the macroscopic boundary condition for the contact angles [14]. Young's law applies in the case where the substrate is perfectly rigid, with elastic modulus $E = \infty$, while Neumann's law holds for liquid lenses floating on another liquid substrate. A question that naturally arises is whether the contact angles vary from "Young" to "Neumann" upon reducing the elastic modulus of the substrate: In other words, does one recover Neumann's angles in the limit $E \to 0$?

Surface deflections due to capillary forces below a drop [10,11,15] have recently been determined with a submicron resolution [16–18]. As reported in Fig. 1(d), Jerison *et al.* [17] demonstrated that the solid exhibits a cusp below the contact line, as would occur for a liquid substrate. In this experiment, however, the solid deformation was found to be ten times smaller than the elastocapillary length γ/E based on the Young modulus E and the liquid surface tension γ. Similarly, the solid angle deflection is much lower than that expected from Neumann's law. Another open question is to identify the dimensionless parameter governing the value of the contact angle or, in other words, to identify the length to which the elastocapillary length γ/E must be compared. This length could be macroscopic, such as the size of the drop [17,19], mesoscopic, or a truly molecular size characteristic for the capillary interactions [20,21]. At what value of γ/E does the elastic substrate develop a cusp?

In this Letter, we solve the elastocapillary contact angle selection within the framework of the density functional theory (DFT), using the sharp-kink approximation. The evolution of the contact angles with stiffness is summarized in Fig. 1. The central result is that the liquid contact angle is selected at the molecular scale a and therefore exhibits a transition from Young to Neumann around a dimensionless number $\gamma/(Ea)$ of order unity. We propose an analytical description of this transition, which agrees quantitatively with the full numerical solution of the coupled DFT and elasticity models. Above this transition, the elastic solid is deformed by the capillary forces over the length γ/E. When the latter becomes larger than the system size [the layer thickness h in Fig. 1(c)], the elastic deformation saturates. Importantly, the soft limit $\gamma/(Ea) \ll 1$ does not reduce to Neumann's law for the contact angles whenever tangential forces are transmitted below the contact line. In this case, the solid cusp is much less sharp than predicted from Neumann's law, which could explain recent experiments.

Density functional theory.—The multiscale nature of elasticity makes it convenient to treat the wetting interactions in a continuum framework, such as the DFT. We consider a simplified DFT model in which the solid and the liquid are treated as homogeneous phases that mutually

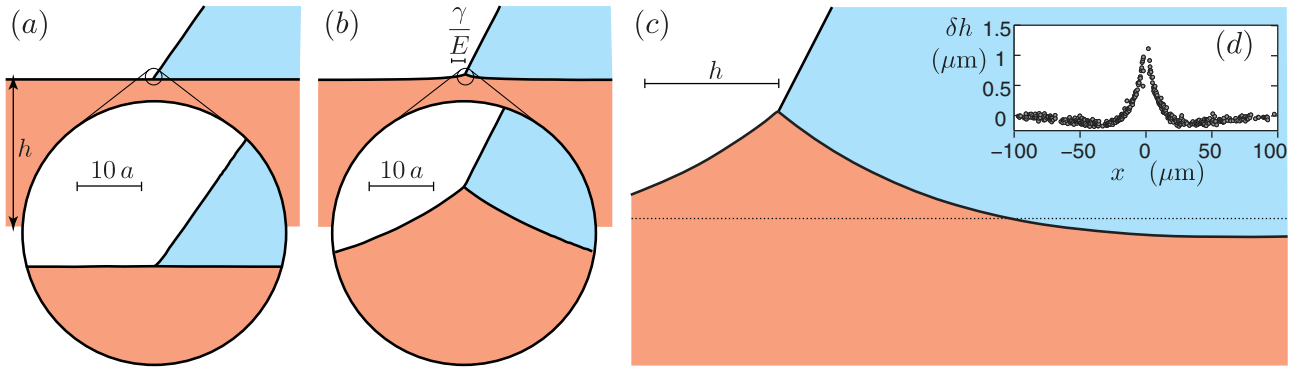

FIG. 1 (color online). Geometry near the three-phase contact line obtained by coupling elasticity to a DFT model. Contact angles continuously vary from Young's law to Neumann's law by reducing the stiffness of the solid. (a) Rigid solid, $\gamma/(Ea) \ll 1$. The surface is undeformed, and the liquid contact angle follows Young's law down to molecular scale a. (b) Soft solid, $\gamma/(Ea) \gg 1$. Surface elasticity is negligible on the scale of molecular interactions, and the contact angles obey Neumann's law. The solid is deformed over a distance $\sim\gamma/E$ from the contact line. (c) Very soft solid, $\gamma/(Eh) \sim 1$. The change of the contact angles saturates when γ/E becomes comparable to the thickness of the elastic film. The solid angle measured at scale h becomes identical to the microscopic solid angle at scale a. (d) Surface elevation profile measured by Jerison *et al.* [17] induced by a water drop on a silicon gel ($E = 3$ kPa). The solid deforms into a "cusp" of solid angle $\theta_S = 164°$.

attract, while the interface is assumed to be infinitely thin [22–24]. This model captures the microscopic properties, such as the stress anisotropy near the interface, the disjoining pressure, and the line tension, and is consistent with macroscopic thermodynamics in the form of Laplace pressure and Young's law [22–25].

The idea underlying this DFT model is to separate the molecular interactions into a long-range attractive potential $\varphi(r)$, which takes into account the pair correlation function, and a hard-core repulsion that acts as a contact force. For van der Waals interactions, this potential decays as $1/r^6$, which is cut off at a microscopic distance $r = a$ that corresponds to the repulsive core. In the model, it turns out that all the capillary forces can be expressed in terms of the integrated potential [21],

$$\Phi_{\alpha\beta}(\mathbf{r}) = \rho_\alpha \rho_\beta \int_\alpha \mathbf{dr}' \varphi_{\alpha\beta}(|\mathbf{r} - \mathbf{r}'|). \tag{1}$$

This represents the potential energy in phase β due to phase α, where the phases can be liquid (L), solid (S), or vapor (V). ρ_α and ρ_β are the corresponding homogeneous densities. The repulsive core at $r = a$ ensures that the integrals over the entire domain α converge and is modeled by an isotropic internal pressure that ensures incompressibility. As detailed in Refs. [21,26], the model distinguishes three types of attractive interactions: liquid-liquid, solid-solid, and solid-liquid interactions, which can be expressed directly in terms of the surface tensions γ, γ_{SV}, and γ_{SL} [21,23,27]. The liquid-vapor surface tension γ characterizes the liquid-liquid interactions. The strength of the solid-liquid interactions is characterized by Young's contact angle θ_Y, defined by $\cos\theta_Y = (\gamma_{SV} - \gamma_{SL})/\gamma$. The interaction with vapor can be neglected in the limit of a low vapor density. In the full DFT numerical calculation, the equilibrium shape of the liquid-vapor interface is determined iteratively using the procedure described in previous papers [24,25].

Selection of the liquid angle.—An important feature is that the strength of the capillary interactions depends on the geometry of the deformable solid. We consider the reference case of a solid shaped like a wedge of angle θ_S (upper inset of Fig. 2). Similar to the case of a flat surface, the force acting on a corner of liquid depends only on its angle θ_L at a large distance from the contact line and can be determined exactly by integrating over all the interactions in the DFT model [23,24]. This force on the liquid corner consists of three contributions that are sketched in the lower inset of Fig. 2: (i) the force exerted by the solid (solid-liquid interactions, black arrow), (ii) the attractive force exerted by the rest of the liquid (liquid-liquid interactions, white arrows), and (iii) the repulsive force exerted by the rest of the liquid, induced by the presence of the solid [28] (liquid-liquid interactions, red arrow). This last force arises because the presence of the solid leads to an increase of the liquid internal pressure near the solid-liquid interface.

The balance of forces in Fig. 2 provides the equilibrium θ_L for arbitrary θ_S (details are worked out in the Supplemental Material [26]):

$$\cos\theta_L = \frac{1}{2}\left(\cos\theta_Y[1 - \cos\theta_S] - \sin\theta_S\sqrt{\frac{2}{1 - \cos\theta_S} - \cos^2\theta_Y}\right). \tag{2}$$

This result is independent of the microscopic length a and the functional form of $\varphi(r)$. For a flat surface ($\theta_S = \pi$), the solid-on-liquid force is oriented vertically, with $f_{SL} = \gamma \sin\theta_L$. In this case, the force balance reduces to Young's

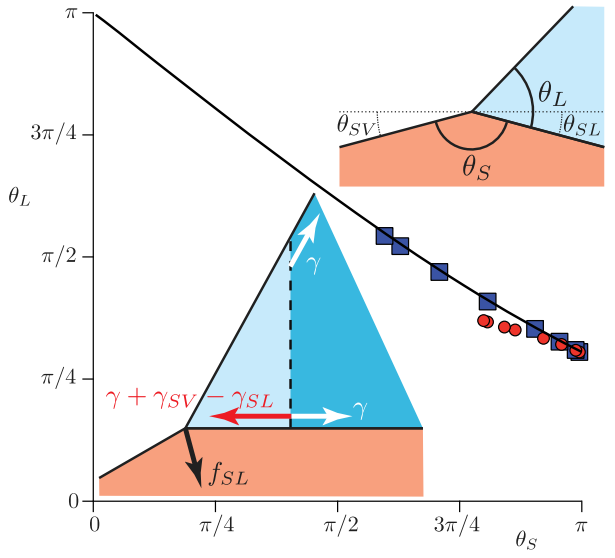

FIG. 2 (color online). Main graph: Relation between θ_L and θ_S predicted by the DFT model. The solid line is the analytic formula (2) for $\theta_Y = 0.96$. The symbols are the angles obtained numerically for the normal force transmission model (■) and the vectorial force transmission model (●), as defined in the text. Upper inset: Definition of θ_L and θ_S. Lower inset: Forces acting on a corner of liquid (bright region, light blue). Black: Force exerted by the solid. Red: Repulsive liquid-liquid force induced by the presence of the solid. White: Attractive force exerted by the liquid due to the missing half-domain of liquid.

law, and the liquid angle $\theta_L = \theta_Y$. However, (2) predicts that θ_L increases when θ_S is reduced (Fig. 2, solid line). Physically, this is due to the reduction of the solid volume for smaller θ_S: This lowers the total solid-liquid interaction, making the solid wedge more "hydrophobic."

Selection of the solid angle.—If the phase S behaves as a perfect liquid, its mechanical equilibrium gives a second equation for the angles. This can be deduced from (2) by exchanging the roles of L and S, which indeed result in θ_S and θ_L, according to Neumann's law [26]. In the elastocapillary problem, by contrast, the solid S can resist shear. One therefore needs to express how the capillary stress $\boldsymbol{\sigma}$ applied at the free surface deforms the solid. We treat the substrate as an incompressible elastic body (Poisson ratio $\nu = 1/2$) with Young's modulus E, as is typical for soft elastomers. We introduce the Green's function $\mathbf{R}$, which gives the surface displacement induced by a Dirac force distribution applied at the boundary of a two-dimensional elastic medium. Then, the total surface displacement is obtained by the convolution

$$\delta h(x) = \frac{1}{E}\int_{-\infty}^{\infty} \mathbf{R}(x - x'; h) \cdot \boldsymbol{\sigma}(x')dx'.$$

The contact line is considered to be invariant in one direction, so that $\mathbf{R}$ and $\boldsymbol{\sigma}$ have two components corresponding to the normal and the tangential directions to the substrate. Let us emphasise that the problem is inherently multiscale. On one hand, the capillary forces are localized in the vicinity of the contact line; on the other hand, the surface displacement induced by a localized force of resultant f_z scales as [29]

$$\delta h(x) \sim -\frac{f_z}{E}\ln|x| \tag{3}$$

and is therefore singular at both small and large distances x from the contact line. The elastic kernel requires a cutoff length at a large scale, which for our numerical calculations arises due to the finite elastic film thickness h [17]. It can also result from the finite size of the drop [20,30,31]. The inner regularization originates from the finite range of intermolecular capillary forces [10,13,21]. The capillary-induced stress $\boldsymbol{\sigma}$ can be expressed in terms of the $\Phi_{\alpha\beta}$ [26], and the integrals of (1) can be evaluated numerically for the arbitrary shape of the liquid and solid domains. This closes the elastocapillary problem, and the resulting numerical profiles are provided in Fig. 1.

At intermediate distances from the contact line, $a \ll x \ll h$, the Green's function for the elastic response is given by Eq. (3). The slope of the solid-liquid interface thus scales as $\delta h' \sim f_z/(Ex)$. Importantly, the angle θ_L of the liquid is selected at the microscale a. Therefore, the relevant solid angle θ_S induced by elastic deformations must be defined at that scale. This is confirmed by the agreement between the prediction of (2) and the numerical solution of the fully coupled elasticity DFT model: The symbols in Fig. 2 are obtained by measuring θ_S in the numerics at a distance a from the contact line. With this information, one can obtain an approximate equation for the selection of θ_S by evaluating (3) at $x = a$:

$$\delta h' \sim \tan\left(\frac{\pi - \theta_S}{2}\right) \sim \frac{f_z}{Ea}. \tag{4}$$

The force acting on the solid corner.—The final step is to express the vertical force f_z exerted on the solid corner in the vicinity of the contact line (bright, light orange region in Fig. 3). Using the approximation that the solid domain is a perfect wedge and assuming that the liquid is at equilibrium, we can derive the tangential and normal components of this force due to the liquid-solid interaction [26],

$$\frac{f^t_{LS}}{\gamma} = (1 + \cos\theta_Y)\frac{\cos\frac{\theta_L}{2}\sin\frac{\theta_S}{2}}{\sin\frac{\theta_L+\theta_S}{2}}, \tag{5}$$

$$\frac{f^n_{LS}}{\gamma} = \frac{(1 + \cos\theta_Y)}{2}\left(\sin\theta_S + \frac{\cos\theta_S}{\tan\frac{\theta_L+\theta_S}{2}}\right) + \frac{(1 - \cos\theta_Y)}{2}\frac{\theta_L}{2}. \tag{6}$$

As emphasized in recent papers, this force is oriented towards the interior of the liquid and therefore presents a large tangential component, even in the limit of a flat surface [21,32].

To express the solid-solid interactions, we need to model the mechanical behavior of the surface layer of the substrate. We consider two extreme cases of how the liquid-on-solid force can be transmitted to the bulk of the elastic solid. First, one can assume that only the normal stress is transmitted, as would be the case for a liquid. In terms of forces on the solid corner (bright region in Fig. 3), the tangential component of f_{LS} is balanced by a surface stress. This is represented by the red arrow in Fig. 3(a) (in perfect analogy to the red arrow in the liquid in Fig. 2). In this case of *normal force transmission*, the total vertical force reads

$$f_z = f^n_{LS}\cos\theta_{SL} + (-f^t_{LS} + \gamma - \gamma_{SL})\sin\theta_{SL} - \gamma_{SV}\sin\theta_{SV}. \quad (7)$$

The angles θ_{SL} and θ_{SV} are defined with respect to the undisturbed solid surface (Fig. 2).

Alternatively, one can hypothesize a perfect *vectorial force transmission*, for which there is no such surface stress [Fig. 3(b)]. We recently proposed an experimental test aiming to discriminate between the two force transmission models: It turned out that the vectorial transmission model is the correct description for an elastomer [32]. Then, the tangential force exerted by the liquid is transmitted to the bulk of the elastic body and the total force on the solid corner becomes [Fig. 3(b)]

$$f_z = f^n_{LS}\cos\theta_{SL} + (-f^t_{LS} - \gamma_{SV})\sin\theta_{SL} - \gamma_{SV}\sin\theta_{SV}. \quad (8)$$

Discussion.—The system of equations (2)–(6), closed by Eq. (7) or Eq. (8), gives a prediction for θ_L and θ_S and forms the central result of our Letter. It involves three dimensionless parameters: the elastocapillary number $\gamma/(Ea)$ and the surface tension ratios γ_{SV}/γ and γ_{SL}/γ. The resulting contact angles are shown as solid lines in Fig. 4 and are in excellent agreement with the numerical solution of the full elasticity DFT model. The contact angles undergo a transition governed by the dimensionless parameter $\gamma/(Ea)$. The relevant length scale that determines the contact angles is therefore microscopic and not macroscopic. In the limit of strong elasticity, $\gamma/(Ea) \ll 1$, one recovers Young's angle $\theta_L = \theta_Y$ and an undeformed solid $\theta_S = \pi$. Conversely, in the limit of a soft solid, for $\gamma/(Ea) \gg 1$, the elasticity is too weak to resist any normal force near the contact line. In this limit, one thus finds that $f_z = 0$, corresponding to a perfect balance of capillary forces. The resulting angles are not only determined by the surface tensions but also depend on the solid surface stress. As expected, Neumann's law is recovered for the *normal force transmission* model [Eq. (7)]. Indeed, in that case, the solid behaves as an incompressible liquid in the limit $\gamma/(Ea) \to \infty$.

For the *vectorial force transmission* model [Eq. (8)], however, the absence of a surface stress changes the force balance along x: A residual horizontal force f_x remains even when $\gamma/E \gg a$. As a consequence, the contact angles are different from Neumann's law. In particular, Fig. 4 reveals that the deflection of the solid, π-θ_S, is significantly smaller than the prediction of Neumann's law. This could be an explanation for the unexpectedly small elastic deformation observed by Jerison *et al.* [17], for which the solid angle was fitted as $\theta_S \approx 164°$ [Fig. 1(d)]. A fully quantitative comparison is not possible at present, since the surface tensions γ_{SV} and γ_{SL} are not known from independent measurements. However, the same experiments revealed significant horizontal displacements below the contact line, consistent with a residual tangential force.

The selection of the contact angle at the scale a has a very important consequence: The strain in the vicinity of

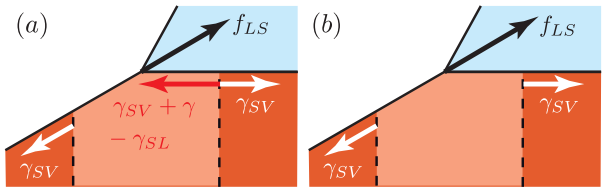

FIG. 3 (color online). Forces acting on the corner of the solid near the contact line [indicated by the bright (light orange) region near the contact line]. (a) Normal force transmission model. Black: Force exerted by the liquid. Red: Force exerted by the solid due to pressure build induced by the liquid. White: Force exerted by the solid due to the missing half-domain of solid. (b) Vectorial force transmission model. The difference with respect to (a) is the absence of surface stress (red).

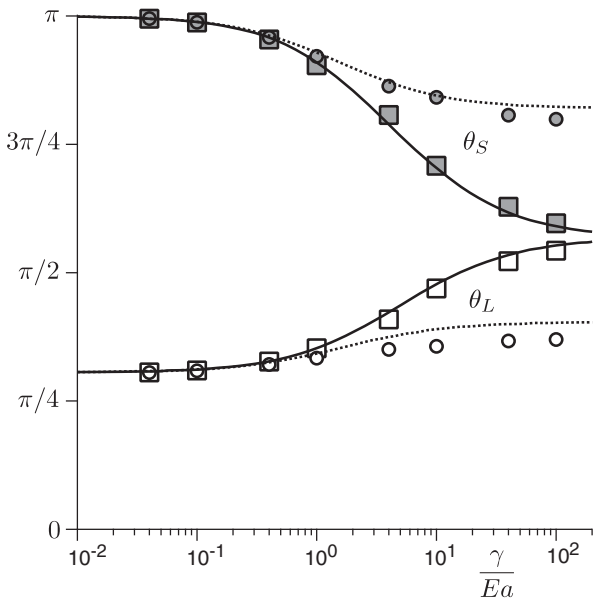

FIG. 4. Transition of the contact angles θ_L (white) and θ_S (gray) upon increasing the "softness" parameter $\gamma/(Ea)$ for $\theta_Y = 0.96$ and $\gamma_{SV} = \gamma$. The symbols correspond to DFT numerical solutions for $h/a = 1000$ for the normal transmission force (□) and for the vectorial transmission force (○).

the contact line scales as $\gamma/(Ea)$. For soft elastomers, this would imply unphysically large strains of 10^3. Clearly, enthalpic effects will become important at large strain, leading to a strengthening of the material [33]. The effective value of $\gamma/(Ea)$ will thus be much smaller than expected from small-strain calibrations. To quantitatively analyze experiments, the effective elasticity must be determined in a self-consistent way in order to describe the strongly strained zone below the contact line.

*Present address: Department of Mechanical Engineering, University of Alberta, Alberta, Canada T6G 2G8.

[1] J. Bico, B. Roman, L. Moulin, and A. Boudaoud, Nature (London) **432**, 690 (2004).
[2] J. W. van Honschoten, J. W. Berenschot, T. Ondaruhu, R. G. P. Sanders, J. Sundaram, M. Elwenspoek, and N. R. Tas, Appl. Phys. Lett. **97**, 014103 (2010).
[3] S. Jung, P. M. Reis, J. James, C. Clanet, and J. W. M. Bush, Phys. Fluids **21**, 091110 (2009).
[4] C. Duprat, S. Protiere, A. Y. Beebe, and H. A. Stone, Nature (London) **482**, 510 (2012).
[5] C. Py, P. Reverdy, L. Doppler, J. Bico, B. Roman, and C. N. Baroud, Phys. Rev. Lett. **98**, 156103 (2007).
[6] J. Bico and B. Roman, J. Phys. Condens. Matter **22**, 493101 (2010).
[7] M. Sokuler, G. K. Auernhammer, M. Roth, C. Liu, E. Bonaccurso, and H.-J. Butt, Langmuir **26**, 1544 (2010).
[8] S. Shojaei-Zadeh, S. Swanson, and S. L. Anna, Soft Matter **5**, 743 (2009).
[9] S. Mora, T. Phou, J.-M. Fromental, L. M. Pismen, and Y. Pomeau, Phys. Rev. Lett. **105**, 214301 (2010).
[10] A. I. Rusanov, Colloid J. USSR **37**, 614 (1975).
[11] S. Yuk and M. Jhon, J. Colloid Interface Sci. **110**, 252 (1986).
[12] M. E. R. Shanahan, J. Phys. D **20**, 945 (1987).
[13] L. R. White, J. Colloid Interface Sci. **258**, 82 (2003).
[14] P.-G. de Gennes, F. Brochard-Wyart, and D. Quere, *Capillarity and Wetting Phenomena: Drops, Bubbles, Pearls, Waves* (Springer, New York, 2003).
[15] C. Extrand and Y. Kumagai, J. Colloid Interface Sci. **184**, 191 (1996).
[16] R. Pericet-Camara, A. Best, H.-J. Butt, and E. Bonaccurso, Langmuir **24**, 10 565 (2008).
[17] E. R. Jerison, Y. Xu, L. A. Wilen, and E. R. Dufresne, Phys. Rev. Lett. **106**, 186103 (2011).
[18] R. W. Style, Y. Che, J. S. Wettlaufer, L. A. Wilen, and E. R. Dufresne, arXiv:1209.3723.
[19] R. W. Style and E. R. Dufresne, Soft Matter **8**, 7177 (2012).
[20] G. R. Lester, J. Colloid Sci. **16**, 315 (1961).
[21] S. Das, A. Marchand, B. Andreotti, and J. H. Snoeijer, Phys. Fluids **23**, 072006 (2011).
[22] T. Getta and S. Dietrich, Phys. Rev. E **57**, 655 (1998).
[23] G. J. Merchant and J. B. Keller, Phys. Fluids A **4**, 477 (1992).
[24] J. H. Snoeijer and B. Andreotti, Phys. Fluids **20**, 057101 (2008).
[25] J. Weijs, A. Marchand, B. Andreotti, D. Lohse, and J. H. Snoeijer, Phys. Fluids **23**, 022001 (2011).
[26] See Supplemental Material at http://link.aps.org/supplemental/10.1103/PhysRevLett.109.236101 for analytical derivations.
[27] C. Bauer and S. Dietrich, Eur. Phys. J. B **10**, 767 (1999).
[28] M. J. P. Nijmeijer, C. Bruin, A. F. Bakker, and J. M. J. Van Leeuwen, Phys. Rev. A **42**, 6052 (1990).
[29] K. L. Johnson, *Contact Mechanics* (Cambridge University Press, Cambridge, England, 1985).
[30] D. J. Srolovitz, S. A. Safran, and R. Tenne, Phys. Rev. E **49**, 5260 (1994).
[31] Y.-S. Yu and Y.-P. Zhao, J. Colloid Interface Sci. **339**, 489 (2009).
[32] A. Marchand, S. Das, J. H. Snoeijer, and B. Andreotti, Phys. Rev. Lett. **108**, 094301 (2012).
[33] M. S. Turner and P. Sens, Biophys. J. **76**, 564 (1999).